Sound propagation in capillary-tube-type porous media with small pores in the capillary walls

W. Patrick Arnott, James M. Sabatier, and Richard Raspet
National Center for Physical Acoustics, and the Department of Physics and Astronomy, University of Mississippi, University, Mississippi 38677

(Received 18 February 1991; revised 24 July 1991; accepted 7 August 1991)

Sound propagation in gas-filled capillary-tube-type porous media was investigated. The capillary tubes were taken to be nominally straight with very small pores in the walls of the capillary tubes. The complex wave number and the characteristic impedance of such media were evaluated. Application to ceramic samples having capillary pores with square cross sections and porous walls is developed as an explanation for the anomalous tortuosity factor previously inferred for this material. Specific acoustic impedance (SAI) measurements were performed for rigid-backed square pore ceramic media having finite wall porosity. It is shown that phase velocity is decreased, attenuation is increased, and characteristic impedance is decreased by finite wall porosity. SAI measurements were also performed after the wall pores were filled with water. These measurements agree favorably with the porous wall and nonporous wall theories, respectively. This work provides a model for the acoustical properties of gas-filled monolithic catalyst supports of which the square pore ceramic media is an example.

PACS numbers: 43.28.Fp, 43.50.Vt, 43.20.Mv

INTRODUCTION

Theory[1,2] and experiments[1] were recently reported for sound propagation in porous media consisting of straight capillary tubes having square cross sections. The experimental work was aimed at testing the efficacy of first-principle models for predicting the acoustical properties of porous media with well-defined geometries. The measured complex wave number[1] was approximately 10% larger than the values predicted from theory assuming nonporous walls. However, the ceramic porous sample used actually has walls that are porous, as indicated schematically in Fig. 1(a) and (b). A qualitative explanation for the discrepancy was that the finite porosity of the ceramic square pore wall should increase the bulk compressibility of air in the porous media and hence increase the complex wave number. This decreases the phase velocity and increases the attenuation, as was observed in the measurements. Effects of wall pores on propagation in porous media were also qualitatively discussed earlier.[3]

In this paper, the effects of finite wall porosity are included in the theory for sound propagation in a porous media consisting of nominally straight capillary tubes with much smaller pores in the capillary tube walls. The theory is cast in a sufficiently general form that it is useful for capillary tubes having geometries other than squares. Specific acoustic impedance (SAI) measurements of a rigid-backed ceramic sample and a previous measurement of the complex wave number[1] compare favorably with the porous-wall porous media theory. Wall pores were filled with water and the SAI measurements were repeated. These measurements agree favorably with nonporous wall theory. The theory shows that the complex wave number is *increased* and the characteristic impedance is *decreased* on account of finite wall porosity.

Finite wall impedance concepts have been used in related work. For a sufficiently wide tube, absorption of the plane wave mode can be accounted for using the expression for boundary layer impedance as a boundary condition at the tube wall.[4] Similarly, sound absorption in ducts with absorbing liners at the duct wall can be modeled using the liner impedance as a boundary condition.[5] These concepts also find use in bore hole measurements in geophysics.[6]

The ceramics used in this investigation are an example of a monolithic catalyst support.[7] Several manufacturers use these ceramics in automobile catalytic converters. Physical properties, such as the ability to hold coatings and low thermal conductivity, can be obtained by adjusting the ceramic wall porosity.[7] A combustible material that burns out during the final sintering is added to the raw ceramic mixture to increase the porosity for some applications.[7] The theory developed here provides a model for the low-frequency acoustical properties of gas-filled monolithic catalyst supports. These ceramics may be useful as low-frequency sound absorbers. They may also be useful in thermoacoustic heat engines due to their low thermal conductivity, regular geometry, wide spread availability, and low cost.

I. PROPAGATION IN POROUS WALL POROUS MEDIA

A. Assumptions

In ideal acoustics an often used approximation is that sound wave propagation is adiabatic and that the fluid is inviscid. At boundaries it is sufficient to assume continuity

[a] This work was presented at the 120th Meeting of the Acoustical Society of America [J. Acoust. Soc. Am. Suppl. 1 **88**, S143 (1990)].

 0001-4966/91/123299-08$00.80

of pressure and the normal component of particle velocity. Ideal acoustics boundary conditions are not sufficient to describe sound propagation in porous media for which the solid and fluid volumes are intermingled and are on the same order. Account must be taken of momentum and energy transport phenomena, viscosity and thermal conductivity, which occur as a result of velocity and temperature gradients. In viscous fluids it is usually a good assumption that the total particle velocity is zero at a rigid stationary boundary. For boundaries such as solid–gas interfaces compression and expansion of gas can result in transport of heat to and from the solid for parcels of gas sufficiently close to the walls. At boundaries gas and solid temperatures are assumed to be the same since in solids the heat capacity is usually much greater than that of the gas. Any local heating of the solid due to the gas is diffused throughout the solid since it is generally a much better heat conductor than the gas.

Dimensionless numbers indicate different regimes of disturbances in porous media. Denote by ρ_0, c_p, η, and κ the gas properties of ambient density, constant pressure heat capacity per unit mass, viscosity, and thermal conductivity. A measure of the relative magnitude of viscous and thermal diffusion in the gas is given by the Prandtl number, $N_{\mathrm{Pr}} = \eta c_p/\kappa$. Gas viscous and thermal penetration depths for oscillations of radian frequency ω are $\delta_\eta = (2\eta/\rho_0\omega)^{1/2}$ and $\delta_\kappa = (2\kappa/\rho_0\omega c_p)^{1/2} = \delta_\eta/N_{\mathrm{Pr}}^{1/2}$, respectively. Denote by R a characteristic transverse pore dimension, e.g., the pore radius for circular pores. A dimensionless shear wave number can be defined as $\lambda = 2^{1/2}R/\delta_\eta = R(\rho_0\omega/\eta)^{1/2}$. Similarly defined for thermal diffusion is a thermal disturbance number $\lambda_T = 2^{1/2}R/\delta_\kappa = R(\rho_0\omega c_p/\kappa)^{1/2} = \lambda N_{\mathrm{Pr}}^{1/2}$. For $\lambda \ll 1$, the magnitude of particle velocity in a pore is much less than that predicted by (inviscid) ideal acoustics and has nearly a quadratic dependence on the transverse coordinates as does dc flow through a capillary tube (Poiseuille flow). For $\lambda \gg 1$, the magnitude of particle velocity closely matches that predicted by ideal acoustics except in a thin boundary layer of thickness δ_η in which particle velocity changes rapidly to zero at the pore wall. For $\lambda_T \ll 1$ the gas temperature is the same as the wall temperature and density changes in the gas occur isothermally rather than adiabatically. For $\lambda_T \gg 1$ density changes are adiabatic except in the thin boundary layer δ_κ surrounding the pore wall over which density changes go from adiabatic to isothermal. A good measure of the characteristic transverse pore dimension is R = twice the transverse pore area/pore perimeter. For example, the characteristic dimension is $R = a$ for circular pores of radius a and for square pores of semiwidth a. This definition of R is twice the hydraulic radius.

Figure 1(a) and (b) represent the model for porous wall porous media. Darkened regions in these figures are the gas-filled portions of the media and the surrounding matrix is taken to be rigid. Plane waves are taken to be propagating in the z direction. Two types of pores are to be distinguished. The main pores are shown to be square in cross section, though this is not necessary for the theory developed below. The walls of the main pores have pores or holes of much smaller radii in them, and the wall pores are of average length d_ω, as shown in Fig. 1(a). Main pores are not connected by wall pores, as indicated in Fig. 1(b). Transverse dimensions in the main pore are given by coordinates (x,y), as indicated in Fig. 1(a).

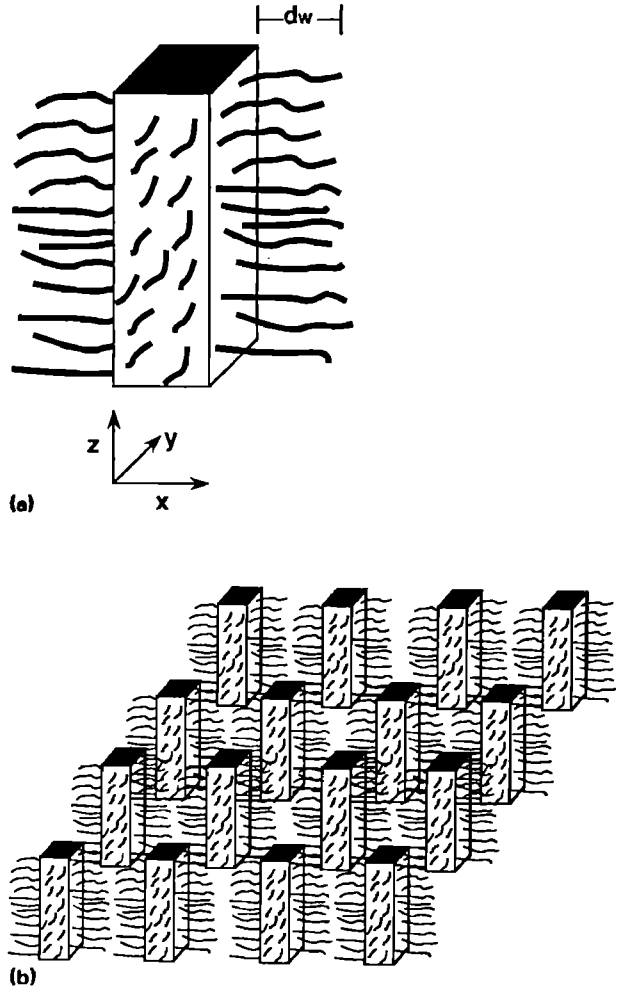

FIG. 1. (a) Single main pore with wall pores of length d_ω. (b) Arrangement of main pores in the porous sample model. Wall pores are not taken to connect adjacent main pores. Air filled regions in (a) and (b) are dark.

The central assumptions are now given concerning oscillatory motion and condensation of gas in the wall pores. At the frequencies considered, particle velocity in the wall pores is much less than it would be for ideal acoustics as a result of gas viscosity and the small radii of wall pores. Condensation of gas in the wall pores is taken to occur isothermally at the same temperature as the solid matrix of the porous media. In terms of the dimensionless parameters, these assumptions are $\lambda_\omega < 1$ and $\lambda_{T\omega} < 1$, where subscript ω refers to wall pores.

The central assumption concerning pressure in the main pore is that it is only a function of the longitudinal coordinate z, not the transverse coordinates.[8] One justification of this assumption is that frequencies considered are much less than the cutoff frequency for radial modes in the main pore. This is the standard assumption for the pressure in nonporous wall porous media theory.[9] A second argument for this assumption is that the wall impedance is much greater than the characteristic impedance in the main pore and the pore diameter is much less than the acoustic wavelength.

The useful range of the porous-wall theory can be stated most generally in terms of the dimensionless numbers relating pore radius and the frequency-dependent viscous penetration depth. This model should be useful for porous media with main pores such that $\lambda > 1$ and wall pores such that $\lambda_w < 1$. These criteria were not derived from more general theory but appear to be consistent with the assumptions made above. In the experiments discussed below $4 < \lambda < 18$ and λ_w was estimated to be in the range $0 < \lambda_w < 1.2$. The frequencies considered were in the range 75–1300 Hz. Wall pore diameters ranged up to $\approx 100\ \mu$m, and the main pore width was 1.54 mm. Further discussion is given in Sec. III.

B. Analysis for porous wall porous media

Consequences of the assumptions given above on the linear acoustic equations in porous wall porous media are now developed. An $\exp(-i\omega t)$ sign convention will be used for constant frequency oscillations. In the frequency domain, linear acoustic quantities in a single main pore are transverse and longitudinal components of particle velocity, $\mathbf{v}(x,y,z) = \mathbf{v}_\tau(x,y,z) + v_z(x,y,z)\hat{z}$, pressure, $p(z)$, density, $\rho(x,y,z)$, and temperature, $T(x,y,z)$. Ambient quantities are density, ρ_0, temperature, T_0, and pressure, p_0. The transverse velocity has been computed for circular pores and nonporous walls by Tijdeman.[10]

A general result is established first. In the geometry of a single main pore in Fig. 1(a), the continuity equation is

$$-i\omega\rho(x,y,z) + \rho_0 \frac{\partial v_z(x,y,z)}{\partial z} + \rho_0 \nabla_\tau \cdot \mathbf{v}_\tau(x,y,z) = 0, \tag{1}$$

where $\nabla_\tau = \partial/\partial x\hat{x} + \partial/\partial y\,\hat{y}$ is the transverse gradient operator. Averaging Eq. (1) over the cross section of an arbitrarily shaped main pore, as shown in Fig. 2,

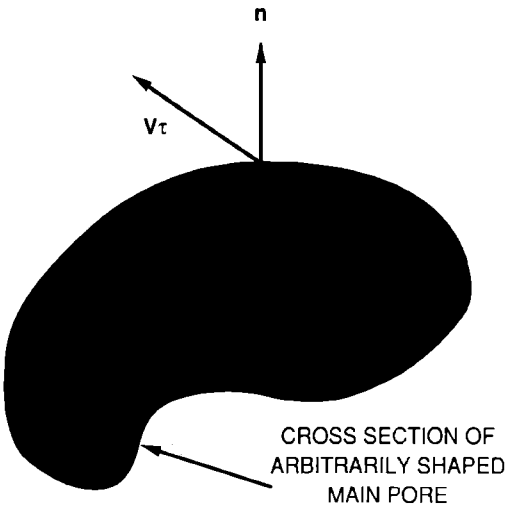

FIG. 2. Arbitrarily shaped cross section of a general main pore having perimeter S and area A. The outward normal is $\mathbf{n}(x,y,z)$ and $\mathbf{v}_\tau(x,y,z)$ is the tangential component of particle velocity. For main pores having square cross sections, as in Fig. 1(a), the cross section would be a square. Wall pores (not shown) are assumed to skirt the main pore.

$$-i\omega\rho(z) + \rho_0 \frac{dv_z(z)}{dz} + \frac{\rho_0}{A}\int_A \nabla_\tau \cdot \mathbf{v}_\tau(x,y,z)\,dx\,dy = 0, \tag{2}$$

where $\rho(z) = A^{-1}\int\rho(x,y,z)\,dx\,dy$ and $v_z(z) = A^{-1}\int v_z \times (x,y,z)\,dx\,dy$ are the cross-sectionally averaged acoustic density and z component of particle velocity for a main pore of cross-sectional area A, e.g., the square area in Fig. 1(a). Application to Eq. (2) of the divergence theorem in the (x,y) plane gives

$$-i\omega\rho(z) + \rho_0 \frac{dv_z(z)}{dz} + \frac{\rho_0}{A}\int_S \mathbf{n}(x,y)\cdot\mathbf{v}_\tau(x,y,z)\,dS = 0, \tag{3}$$

with S being the perimeter of a main pore having outward unit normal $\mathbf{n}$ and dS an element of perimeter. In the standard approach to capillary-tube-based porous models, the main pore wall is both rigid and nonporous and the boundary condition $\mathbf{v}_\tau = 0$ at the pore wall significantly simplifies the pore-averaged continuity equation to $-i\omega\rho(z) + \rho_0\, dv_z(z)/dz = 0$.

According to Eq. (3) average gas density in the main pore changes in time due to compression of the gas and as a result of mass flux $\rho_0\mathbf{n}(x,y)\cdot\mathbf{v}_\tau(x,y,z)$ into the pore wall. A reasonable assumption is that the porous wall radius of curvature in a transverse plane is much greater than typical wall pore diameters. Under this assumption the porous wall can be taken locally to be a flat surface having a specific acoustic impedance Z_w. In this averaged sense continuity of the normal component of $\mathbf{v}_\tau$ (Fig. 2 shows the normal) at the main-pore porous-wall boundary is taken to be

$$\mathbf{n}(x,y)\cdot\mathbf{v}_\tau(x,y,z) = p(z)/Z_w. \tag{4}$$

Here $p(z)/Z_w$ is the *longitudinal particle velocity* in the *wall pores* evaluated at the interface of the main pore and entrance to the wall pores. As discussed above, $p(z)$ is taken to be constant in a given cross section of a main pore. Use of the boundary condition, Eq. (4), in the continuity equation, Eq. (3), gives

$$-i\omega\rho(z) + \rho_0 \frac{dv_z(z)}{dz} + \frac{\rho_0 p(z)}{Z_w}\frac{S}{A} = 0, \tag{5}$$

where S is the perimeter of the arbitrarily shaped main pore, e.g., the square in Fig. 1(a).

Other relations among the acoustic quantities are provided by momentum, state, and heat flow equations. The z component of the momentum equation in a single main pore is[1]

$$-i\omega\rho_0 v_z(x,y,z) = -\frac{dp(z)}{dz} + \eta\nabla_\tau^2 v_z(x,y,z). \tag{6}$$

The boundary condition for Eq. (6) is $v_z(x,y,z) = 0$ for x and y on the nominal location of the main pore boundary. This boundary condition assumes that the *transverse particle velocity* in the *wall pores* is zero since wall pore diameters are much less than the viscous penetration depth. The solution of Eq. (6), when averaged over the cross section of the main pore, as was done above for the continuity equation, is written symbolically as[1]

$$i\omega\rho_0 v_z(z) = F(\lambda)\frac{dp(z)}{dz}, \tag{7}$$

where $F(\lambda)$ is a complex pore-geometry-dependent function that defines a complex density $\rho_0/F(\lambda)$ for gas in the main pore. Recall that $\lambda = R(\rho_0\omega/\eta)^{1/2}$, where $R = 2A/S$. For main pores having rectangular cross sections of semiwidths a and b, $R = 2ab/(a+b)$,

$$Y_{mn}(\lambda) = 1 + (i\pi^2/\lambda^2)[(b^2m^2 + a^2n^2)/(a+b)^2], \tag{8}$$

and the function $F(\lambda)$ is[1,2]

$$F(\lambda) = \frac{64}{\pi^4}\sum_{m,n\ \text{odd}}\frac{1}{m^2n^2Y_{mn}(\lambda)}. \tag{9}$$

The odd integers m and n in Eq. (9) range from 1 to ∞. Note that λ and hence $F(\lambda)$ is a function of a/b for rectangular pores.

Density changes in the wall pores are taken to occur isothermally, as discussed above. Excess temperature goes to zero at the nominal location of the main pore boundary, which is the usual boundary condition. The heat equation and equation of state can be combined to obtain an expression for the excess density in the main pore.[1] Averaging the excess density over the pore cross section gives[1]

$$\rho(z) = \{[\gamma - (\gamma-1)F(\lambda_T)]/c^2\}p(z), \tag{10}$$

where c is the adiabatic sound speed, γ is the ratio of specific heats, and $F(\lambda_T)$ is given by Eq. (9) for rectangular pores and argument $\lambda_T = N_{Pr}^{1/2}\lambda$. For wide main pores such that $\lambda_T \to \infty$, $F(\lambda_T)\to 1$ so that compressions are adiabatic and $\rho(z) = p(z)/c^2$. For narrow main pores such that $\lambda_T \to 0$, $F(\lambda_T)\to 0$ so that compressions are isothermal and $\rho(z) = p(z)/(c^2/\gamma)$. Use of Eq. (10) in the averaged continuity equation, Eq. (5), gives

$$-i\omega\left(\frac{\gamma-(\gamma-1)F(\lambda_T)}{c^2} + \frac{2i\rho_0}{R\omega Z_w}\right)p(z) + \rho_0\frac{dv_z(z)}{dz} = 0, \tag{11}$$

where $R = 2A/S$ was used.

The model is shown in Fig. 1(b) for a bulk porous media consisting of N main pores per unit area, each having cross-sectional area A. *The area A and porosity $\Omega = NA$ are to be measured, assuming that no wall pores are present.* For completeness, allow each main pore to also have a tortuosity q. In the present context, q allows for the possibility of a gentle longitudinal curvature of each main pore, or a tilt angle θ of the main pore axis for which $q = 1/\cos\theta$. Bulk acoustical equations for porous media are obtained by using $V_{zb}(z) = \Omega v_z(z)/q$ and by replacing dz with $q\,dz$.[1] Here $V_{zb}(z)$ is a bulk particle velocity averaged over unit cross section of porous sample. Resulting bulk equations are from Eq. (7),

$$i\omega\rho_0\frac{q}{\Omega}V_{zb}(z) = F(\lambda)\frac{dp(z)}{q\,dz}, \tag{12}$$

and from Eq. (11),

$$-i\omega\left(\frac{\gamma-(\gamma-1)F(\lambda_T)}{c^2} + \frac{2i\rho_0}{R\omega Z_w}\right)p(z) + \rho_0\frac{q}{\Omega}\frac{dV_{zb}(z)}{q\,dz} = 0. \tag{13}$$

Multiplying Eq. (13) by $(i\omega)$, taking d/qdz of Eq. (12), and eliminating $V_{zb}(z)$ from the resulting equations gives an equation for pressure waves of constant frequency,

$$\frac{d^2p(z)}{dz^2} + \frac{\omega^2}{(c/q)^2}\frac{\gamma-(\gamma-1)F(\lambda_T)}{F(\lambda)} \times\left(1 + \frac{c}{\gamma-(\gamma-1)F(\lambda_T)}\frac{2i}{\omega R\zeta_w}\right)p(z) = 0, \tag{14}$$

where $\zeta_w = Z_w/\rho_0 c$ is the normalized wall specific acoustic impedance.

The complex wave number and characteristic impedance of porous wall porous media are obtained from Eq. (14) and Eq. (12). Assuming $p \propto \exp(ikz)$, Eq. (14) yields a dispersion relation for the complex wave number k,

$$k = \pm k_{np}\xi, \tag{15}$$

where

$$k_{np} = [\omega/(c/q)]\sqrt{[\gamma-(\gamma-1)F(\lambda_T)]/F(\lambda)}, \tag{16}$$

is the propagation constant for *nonporous* main-pore walls and

$$\xi \approx 1 + c/[\gamma-(\gamma-1)F(\lambda_T)](i/\omega R\zeta_w), \tag{17}$$

where a binomial expansion for the square root was applied because $\zeta_w \gg 1$. From Eq. (12) the normalized characteristic impedance $\zeta = Z/\rho_0 c$ of the material is

$$\zeta = \zeta_{np}\xi^{-1}, \tag{18}$$

where

$$\zeta_{np} = \frac{1}{F(\lambda)^{1/2}}\frac{q}{\Omega}\frac{1}{\sqrt{\gamma-(\gamma-1)F(\lambda_T)}}, \tag{19}$$

is the impedance for *nonporous* main-pore walls[1] and

$$\xi^{-1} \approx 1 - c/[\gamma-(\gamma-1)F(\lambda_T)](i/\omega R\zeta_w). \tag{20}$$

Recall that ζ_w is the normalized wall specific acoustic impedance.

The model illustrated in Fig. 1(a) and (b) assumes wall pores are of length d_w and terminate in the pore wall. A reasonable model for wall impedance is a rigid-backed layer model with $\zeta_w = i\zeta_{cw}\cot(k_w d_w) \approx i\zeta_{cw}/(k_w d_w)$, where the cotangent approximation applies when $k_w d_w \ll 1$, k_w is the propagation constant for the wall pores, and ζ_{cw} is the normalized characteristic impedance of the wall. An impedance model for sufficiently low frequency and wall pores with geometries such that $\lambda_w < 1$ has $k_w = q_w\omega(8i\gamma)^{1/2}/(c\lambda_w)$ and $\zeta_{cw} = q_w(8i/\gamma)^{1/2}/(\Omega_w\lambda_w)$, where q_w and Ω_w are the tortuosity of wall pores and the porosity of the wall.[11] Wall porosity Ω_w is defined as the open volume in the walls divided by the total volume of the walls. Combining these expressions gives a wall-pore normalized specific acoustic impedance that is independent of λ_w,

$$\zeta_w \approx ic/\omega\gamma\Omega_w d_w. \tag{21}$$

Use of Eq. (21) in Eq. (17) gives

$$\xi \approx 1 + \frac{\gamma}{\gamma - (\gamma - 1)F(\lambda_T)} \frac{\Omega_w d_w}{R}$$

$$= 1 + \frac{\gamma}{\gamma - (\gamma - 1)F(\lambda_T)} \frac{\Omega_T - \Omega}{2\Omega}, \quad (22)$$

where in the second form, the total porosity Ω_T is the total open volume (wall-pore volume plus main pore volume) divided the total sample volume. Equation (22) was obtained using the relation

$$\Omega_T = \Omega(1 + 2\Omega_w d_w/R). \quad (23)$$

The total porosity Ω_T can be obtained from Eq. (23) by measuring Ω and R, and by optimizing agreement between theory and experiment to obtain Ω_w and d_w. This is discussed further in Sec. III.

For main pores large enough that $\lambda_T \gg 1$ so that $F(\lambda_T) = 1$, $\xi > 1$ is a real quantity. Consequences of $\xi > 1$ are seen in Eq. (15) and the definition $k = \omega/c_{ph} + i\alpha$, where c_{ph} is the phase velocity and α is the attenuation constant. Attenuation is increased by $\xi > 1$ and phase velocity decreased, and by Eq. (18) the characteristic impedance is decreased. The factor $\gamma/[\gamma - (\gamma - 1)F(\lambda_T)]$ may be attributed to the difference in compressibility of gas in the main pore and much smaller wall pores. Acoustical methods for determining the ratio $(\Omega_T - \Omega)/\Omega$ occurring in Eq. (22) may be of interest in nondestructive evaluation of materials.

The normalized specific acoustic impedance ζ_{rb} of a rigid-backed square pore sample is

$$\zeta_{rb} = i\zeta \cot(kL), \quad (24)$$

where L is its length. Calculations of ζ_{rb} will be compared with measurements in Sec. III. It is noteworthy that this measurement is sensitive to both the characteristic impedance ζ and the complex wave number k of the material when absorption over length $2L$ is not severe.

II. SPECIFIC ACOUSTIC IMPEDANCE MEASUREMENTS

The ceramic porous material has straight tubes with square cross sections, as shown schematically in Fig. 3. The side of the ceramic facing the impedance tube was flush mounted into an aluminum disk of thickness 1.27 cm. Another solid aluminum disk of the same thickness had a hole of depth 0.32 cm and diameter of 14.6 cm machined into it so that the ceramic could be attached. The ceramic and aluminum pieces were attached using epoxy. The solid aluminum disk acts as a rigid termination for the sample. An O ring was machined into the open disk to form a seal with the impedance tube. Threaded rod not shown in Fig. 3 was bolted between the aluminum pieces to add structural support. The outer ceramic surface was sealed against leaks by covering it with polyurethane.

Specific acoustic impedance (SAI) measurements were made on a square pore ceramic sample having a nominal cell density of $C = 200$ pores/in.^{2}, average square pore semiwidth a of 0.768 mm $\pm$ 0.01 mm, and length L of 49.5 cm. Porosity associated with main pores using $\Omega = C(2a)^2 = 73\%$. This value of porosity was computed assuming nonporous walls, as dictated by the theory in Sec. I. Wall thickness was $\approx$0.27 mm. The value $a = 0.77$ mm was used in the calculations. The uncertainty in a was computed from the standard error of 25 measurements.

After SAI measurements were made on the dry, porous wall sample, the ceramic was flooded with water. Strong molecular attraction between water molecules and the ceramic held water in the small volumes of the wall pores. However, water in the main pores was easily removed by shaking the sample. Thus a three phase (water, ceramic, and air) sample was produced. Because of the huge impedance mismatch though, the combination of wall-pore water and ceramic sample wall are considered a rigid matrix. This combination gave us an ideal porous sample consisting of straight, square-pore capillaries *with nonporous walls*. SAI measurements were also made on this three-phase sample.

Figure 4 shows a representative optical microscope photograph from several that were taken of the pore walls.

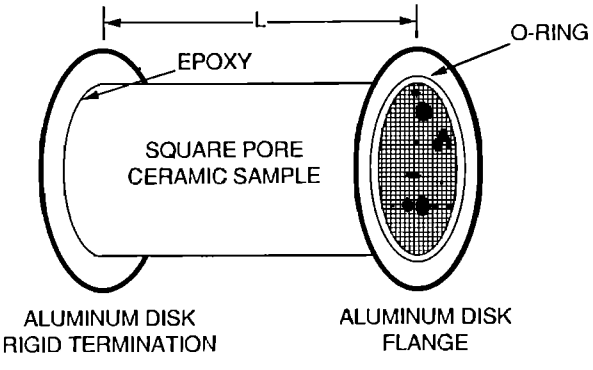

FIG. 3. Arrangement of ceramic sample and aluminum support disks. Threaded rod standoffs were used between the aluminum disks to add structural support. Impedance measurements were made with the ceramic sample attached to the impedance tube in Fig. 5.

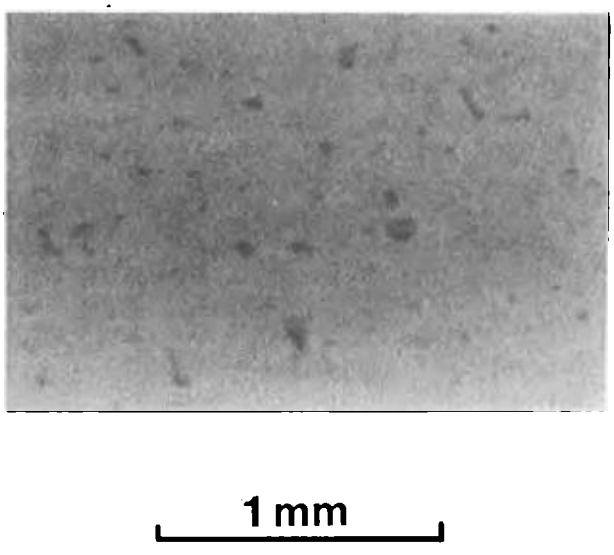

FIG. 4. Representative optical microscope photograph of the porous ceramic wall.

Clearly the ceramic sample has finite wall porosity. The larger pore diameters were estimated to be 100 μm. The interior wall pore volume is roughly spherically shaped, though the walls are not smooth. Wall pores with small diameters in Fig. 4 often open to larger diameter cavities in the ceramic walls. Wall porosity was estimated to be $\Omega_w = 49\%$ by maximizing agreement between the experimental impedance measurement and the theoretical expression, which is a function of Ω_w. An estimate of $d_w = 100\,\mu$m, the depth of wall pores, as shown schematically in Fig. 1(a), was made using a profileometer. The estimated values of Ω_w and d_w will be used in Sec. III to compute the total sample porosity from use of Eq. (23). It appeared that wall pores do not connect by air adjacent main pores.

An impedance tube shown schematically in Fig. 5 was used to measure the specific acoustic impedance of a rigid-backed ceramic sample shown schematically in Fig. 3. Impedance tube design criteria and theory of operation are described elsewhere.[12,13] A dynamic signal analyzer was used in a swept sine mode to drive a power amplifier that was connected to the Altec driver. Denote by H_{1i} the transfer function between microphones M1 and M2 in Fig. 5. The analyzer was also used to measure H_{1i}. The frequency range of interest was 75–1300 Hz, and the cutoff frequency for radial modes in the tube was approximately 1375 Hz. The analyzer was interfaced with a minicomputer to download H_{1i} for the impedance calculation. A transfer function H'_{1i} is measured and the measurement is repeated with the microphones reversed, obtaining H''_{1i}. Since the transfer function used in the calculation is $H_{1i} = (H'_{1i}/H''_{1i})^{1/2}$ the frequency response of each microphone cancels so that one need not be overly concerned with the microphone frequency response or calibration.

III. DISCUSSION OF EXPERIMENTAL AND CALCULATED COMPLEX WAVE NUMBER AND SPECIFIC ACOUSTIC IMPEDANCE

The complex wave number for $C = 200$ pores/in.^{2} ceramic samples was previously measured using a time domain technique. Experimental results are shown in Fig. 6(a) and (b) for phase velocity and attenuation constant. Also shown are theoretical results for porous-wall porous media theory [Eqs. (15) and (22)] and nonporous-wall theory [Eq. (16)]. Porous-wall theory results agree much more favorably with experimental points than the nonporous-wall theory. Porous-wall theory underestimates the attenuation constant though, particularly at higher frequencies. In previous work it was noted that use of an anomalous tortuosity $q = 1.1$ [in the nonporous-wall theory Eq. (16)] was necessary to obtain satisfactory agreement among theoretical and measured values of the complex wave number. This value of tortuosity is anomalous since porous media consisting of straight, rigid, nonporous capillary tubes, which was the model being used, has $q = 1$. The slightly frequency-dependent complex factor computed from Eq. (22) is $\xi \approx 1.1$. This theoretical justification for multiplying the complex wave number by a nonunity factor ξ, even though the capillary tubes are straight, is a main result of this paper.

Measured and calculated specific acoustic impedance are shown in Fig. 7, with the real part in Fig. 7(a) and the imaginary part in Fig. 7(b). The theoretical expression for a

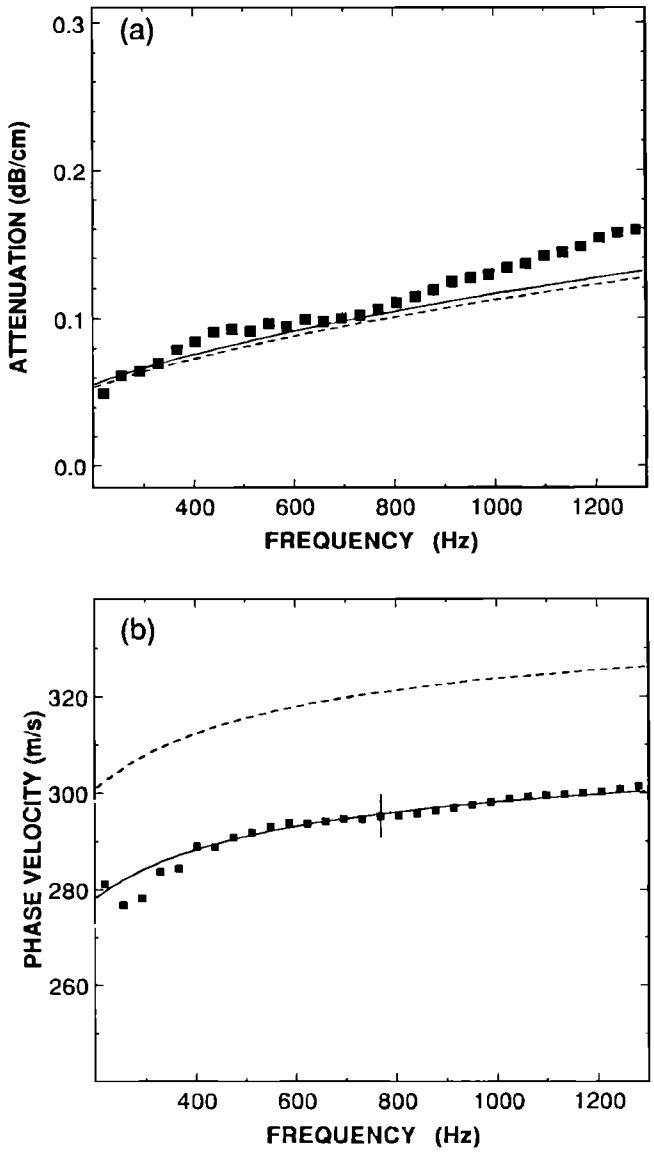

FIG. 6. (a) Attenuation constant and (b) phase velocity measurements and theory. The solid symbols are experimental results for ceramic square pore samples. Error bars were estimated to be twice the symbol size in (a) and a representative error bar is shown in (b). Solid lines and broken lines are porous-wall and nonporous-wall porous-media theory.

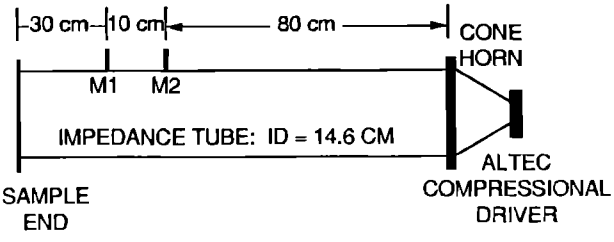

FIG. 5. Impedance tube geometry.

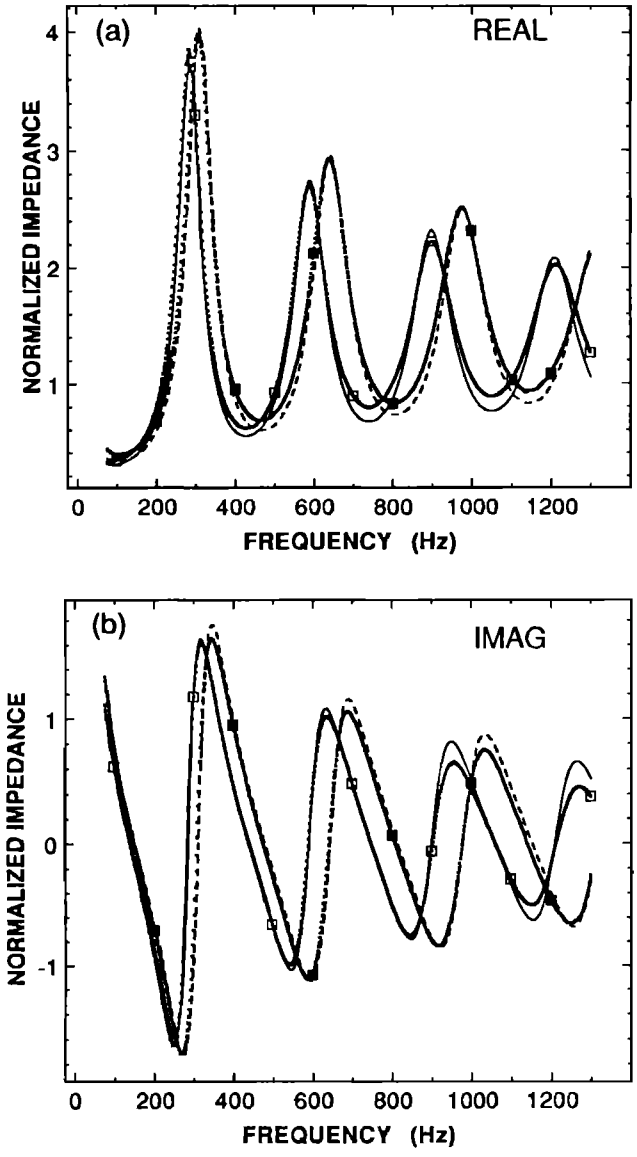

FIG. 7. (a) Real and (b) imaginary specific acoustic impedance measurements and theory. Experimental measurements are given by small squares, which nearly form a continuous curve. Measurements with the wall pores filled with water are marked with large, solid squares. These measurements agree favorably with the nonporous-wall theory given by the dashed lines. Measurements and theory for porous walls are marked with open squares and solid lines, respectively.

rigid-backed sample is given by Eq. (24). Impedance was normalized by the characteristic impedance of air. Constructive and destructive interference of downgoing and upgoing waves in the ceramic sample results in the obvious structure on the impedance curves. Nonporous-wall theory was computed from the use of Eq. (19), and porous-wall theory from Eq. (18) and Eq. (22). With the wall pores filled with water, SAI measurements agree favorably with nonporous-wall theory. When the wall pores are open SAI measurements agree favorably with porous wall theory. The location of peaks and minima agree favorably; however, the computed impedance is less than the measured impedance near minima of the real part. Part of this discrepancy may be attributed to boundary layer absorption on the rigid termination of the ceramic sample: This is not accounted for in Eq. (24). Porous-wall theory gives an impedance greater than the measured impedance for higher frequencies. This is consistent with phase velocity and attenuation measurements shown in Fig. 6, since the frequency of impedance maxima and minima is governed primarily by the phase velocity and the impedance magnitude is governed by the attenuation constant. The assumptions made in Sec. I A for developing the porous-wall porous-media theory are less valid for higher frequencies, since $\lambda_w \approx 1.2$.

Wall porosity Ω_w was used as an adjustable parameter in Eq. (22) to obtain the theoretical wall porosity SAI curves in Fig. 7(a) and (b). Champoux and Stinson measured,[14] using an air-based system,[15] the total porosity Ω_T of a ceramic sample of the same type used in our measurements. Use of Eq. (23) gives $\Omega_T = 0.82$, which is in acceptable agreement with the value $\Omega_T = 0.87 \pm 0.05$ determined by Champoux and Stinson.

In previous work, we referred to the effects of finite wall porosity as an "anomalous tortuosity factor." This notion is incorrect, for by Eq. (19), the characteristic impedance is proportional to tortuosity q. Thus characteristic impedance should increase if finite wall porosity simply caused the tortuosity to increase. Finite wall porosity increases the bulk compressibility of gas in the pores. Since the complex wave number (characteristic impedance) are proportional (inversely proportional) to the square root of compressibility, they increase (decrease) on account of finite wall porosity, as shown quantitatively in Eq. (15) [Eq. (18)].

IV. CONCLUSION

A theory has been developed for propagation in capillary-tube-type porous media in which the capillary tubes have small pores in the walls. The wall pores were modeled as a thin-layered impedance at the main pore wall. The wall impedance was taken to be reactive with the reactance due to small wall pores. Phase velocity is decreased, attenuation is increased, and characteristic impedance is decreased on account of finite wall porosity. Specific acoustic impedance measurements on a ceramic sample having both porous and nonporous walls agree favorably with the calculated values for these two cases. This model may be useful for sound propagation in soils having large cracks and for evaluating the walls of tubes that are susceptible to damage by pitting. This work offers an explanation for the anomalous tortuosity factor, which was used previously[1] for the square pore ceramic samples.

ACKNOWLEDGMENTS

We are grateful to Heui-Seol Roh and Henry E. Bass for their comments and suggestions, to Yvan Champoux and Michael R. Stinson for porosity measurements of our ceramic samples and to Brett Bolen for assistance with impedance tube measurements. Portions of this work were funded by the United States Department of Agriculture, the Office of Naval Research, and the U.S. Army Construction Engineering Research Laboratory.

[1] H. S. Roh, W. P. Arnott, J. M. Sabatier, and R. Raspet, "Measurement and calculation of acoustic propagation constants in arrays of small air-filled rectangular tubes," J. Acoust. Soc. Am. **89**, 2617–2624 (1991).
[2] M. Stinson, "The propagation of plane sound waves in narrow and wide circular tubes, and generalization to uniform tubes of arbitrary cross-sectional shape," J. Acoust. Soc. Am. **89**, 550–558 (1991).
[3] C. Zwikker and C. W. Kosten, *Sound Absorbing Materials* (Elsevier, Amsterdam, 1949), pp. 21 and 125.
[4] A. D. Pierce, Acoustics: *An Introduction to Its Physical Principles and Applications* (Acoustical Society of America, New York, 1989), pp. 532–534.
[5] P. M. Morse, *Vibration and Sound* (American Institute of Physics, New York, 1976), p. 371.
[6] J. E. White, *Underground Sound: Application of Seismic Waves* (Elsevier, New York, 1983), pp. 151–154.
[7] J. J. Burton and R. L. Garten, *Advanced Materials in Catalysis* (Academic Press, New York, 1977), Chap. 10.
[8] Equation (31.4), p. 371 of Ref. 5 shows that the principal mode in ducts with absorbing liners is not a perfect plane wave because the pressure amplitude depends on the transverse coordinates [x,y coordinates in Fig. 1(a)]. The transverse variation can be shown to be negligible in the limit of large wall impedance and small ratio of pore diameter to acoustic wavelength.
[9] See Figs. 2 and 3 in Ref. 2.
[10] H. Tijdeman, "On the propagation of sound waves in cylindrical tubes," J. Sound Vib. **39**, 1–33 (1975).
[11] This model is discussed in Ref. 4, p. 537. Use has been made of the definition of $\lambda_\omega = (\rho_0\omega/\eta)^{1/2}a_\omega$, where a_ω is the wall pore radius assumed to be circular here. The normalized specific acoustic impedance ζ_ω is that of a narrow short tube of length d_ω for isothermal sound speed $c/\gamma^{1/2}$. Also see L. L. Beranek, *Acoustics* (American Instutute of Physics, New York, 1986), pp. 34–35.
[12] A. F. Seybert and D. F. Ross, "Experimental determination of acoustic properties using a two-microphone random-excitation technique," J. Acoust. Soc. Am. **61**, 1362–1370 (1977).
[13] J. Y. Chung and D. A. Blaser, "Transfer function method of measuring in-duct acoustic properties. I. Theory," J. Acoust. Soc. Am. **68**, 907–913 (1980).
[14] Y. Champoux (private communication, 1991).
[15] Y. Champoux, M. R. Stinson, and G. A. Daigle, "Air-based system for the measurement of porosity," J. Acoust. Soc. Am. **89**, 910–916 (1991).